A MILLING CROWD MODEL FOR LOCAL AND LONG-RANGE OBSTRUCTED LATERAL DIFFUSION

Mobility of Excimeric Probes in the Membrane of Intact Erythrocytes

JOSEF EISINGER, JORGE FLORES, AND WESLEY P. PETERSEN
AT&T Bell Laboratories, Murray Hill, New Jersey 07974

ABSTRACT A new model for lateral diffusion, the milling crowd model (MC), is proposed and is used to derive the dependence of the monomeric and excimeric fluorescence yields of excimeric membrane probes on their concentration. According to the MC model, probes migrate by performing spatial exchanges with a randomly chosen nearest neighbor (lipid or probe). Only nearest neighbor probes, one of which is in the excited state, may form an excimer. The exchange frequency, and hence the local lateral diffusion coefficient, may then be determined from experiment with the aid of computer simulation of the excimer formation kinetics. The same model is also used to study the long-range lateral diffusion coefficient of probes in the presence of obstacles (e.g., membrane proteins). The dependence of the monomeric and excimeric fluorescence yields of 1-pyrene-dodecanoic acid probes on their concentration in the membranes of intact erythrocytes was measured and compared with the prediction of the MC model. The analysis yields an excimer formation rate for nearest neighbor molecules of $\sim 1 \times 10^7\ s^{-1}$ and an exchange frequency of $\gtrsim 2 \times 10^7\ s^{-1}$, corresponding to a local diffusion coefficient of greater than $3 \times 10^{-8}\ cm^2\ s^{-1}$. This value is several times larger than the long-range diffusion coefficient for a similar system measured in fluorescence photobleaching recovery experiments. The difference is explained by the fact that long-range diffusion is obstructed by dispersed membrane proteins and is therefore greatly reduced when compared to free diffusion. The dependence of the diffusion coefficient on the fractional area covered by obstacles and on their size is derived from MC simulations and is compared to those of other theories lateral diffusibility.

INTRODUCTION

Just as it is becoming apparent that the dynamical structure of proteins must be included in a complete description of enzyme action, so a knowledge of the dynamical properties of lipid bilayers is necessary for an understanding of the complex architecture and diverse functions of the cell membrane. Recent experiments suggest, for example, that the lateral diffusion of redox components limits and possibly controls the rate of mitochondrial electron transfer (1). Since the mobility of the various membrane components depends on the fluidity of the lipid matrices, many workers have during the past decade studied the rotational and translational mobility of fluorescent (or spin-labeled) lipid analogue probes in a variety of membrane systems. The translational fluidity of model membranes and cells has been measured principally by two experimental methods, both of which employ fluorescent lipid analogue probes. The first, and by far the most widely used method, is fluorescence photo-bleaching recovery (FPR), in which the diffusive motion of fluorescent membrane probes into a region (diameter $\gtrsim 1\ \mu m$) that had previously been bleached by means of a focussed laser beam, is measured (2-4). In the second method, employed largely by Vanderkooi, Sackmann, Galla and their coworkers (5–9), the diffusion-limited rate of excimer (i.e. *excited dimer*) production is measured for excimeric membrane probes. The fluorophore of choice is usually pyrene and the probes' lateral mobility in the membrane is estimated from the observed excimer formation rate.

Several previous analyses, by which the diffusibility of excimeric membrane probes is derived from their excimerization rate, employed a theory which was originally intended for the calculation of exciton trapping rates. We propose here a more general and realistic computer simulation model to relate the molecular dynamics of membrane lipids to the kinetics of excimer formation. This so-called milling crowd model permits the determination of the lateral diffusion coefficient of excimeric probes from their excimeric to monomeric fluorescence yields, measured for a range of probe to phospholipid ratios.

When comparing diffusion coefficients obtained by FPR and by means of excimeric probes, it must be remembered that the characteristic diffusion length differs greatly in these two experimental techniques, being of the order of a

Dr. Petersen's present address is Boeing Computer Services, Tukwila, WA, 98188

micrometer in the former, but $\lesssim$10 nm in the latter. The difference in experimental diffusion lengths becomes important when the lateral mobility of probes in real membranes, as opposed to homogeneous phospholipid vesicle systems, are considered: for in biological membranes, diffusion over large distances is obstructed by protein dispersed in the phospholipid matrix. We have employed a modified version of the milling crowd model to compare obstructed and unobstructed diffusion in two dimensions. It will be seen that when the fractional membrane area occupied by proteins is of the order of a half, as it is in erythrocytic and many other membranes, the diffusion coefficient for obstructed diffusion is reduced relative to "free" diffusion by large factors that depend on the size and number of obstacles. These results, which suggest that the distribution of membrane proteins plays an important and often a dominant role in determining a membrane probes' diffusive behavior, are discussed in relation to existing theories of lateral diffusion (10, 11).

We also report the experimental monomeric and excimeric yields of 1'-pyrenedodecanoic acid in the membranes of intact erythrocytes and use the milling crowd model to obtain the lateral diffusion coefficient for this system.[1]

MATERIALS AND METHODS

Blood samples were obtained from healthy casual donors. After separating the erythrocytes they were washed and suspended in 10 mM/l phosphate buffer, containing 120 mM/l NaCl and 2.7 mM/l KCl, pH 7.4 (PBS). 1'-pyrenedodecanoic acid (PDA) (Molecular Probes, Junction City, OR) was used without further purification and after wetting with tetrahydrofuran was dissolved in ethanol at a concentration of about 5 mg/ml, the exact concentration being determined by an absorption measurement, using 4.0×10^4 as the molar extinction coefficient at 342 nm. Erythrocytes were labeled by adding microliter quantities of the PDA stock solution to 2.5 ml of a red cell suspension at a hematocrit of 0.2, at room temperature while stirring. The efficiency of PDA incorporation was measured (13) by comparing the PDA fluorescence intensity of this incubation mixture after adding 1% sodium dodecyl sulfate (SDS), to lyse the cells and incorporate PDA in SDS micelles and then comparing it to the PDA signal from the washed erythrocytes, after again adding SDS. More than 95% of the PDA were found to remain in the RBC membranes for molar probe ratios as high as 0.3. Probe ratios were calculated from the number of PDA molecules in the incubation mixture and its hematocrit, using 1.15×10^{10} ml^{-1} for the concentration of packed erythrocytes and 2.2×10^8 for the number of lipid molecules (including cholesterol) in the outer leaflet of each erythrocyte (14, 15).

It is remarkable that erythrocytes can accommodate fatty acids corresponding to a probe ratio as high as one third in their membranes, with echinocytosis being prominent only at probe ratio's greater than ~10% but depending on the buffer. Phosphotidylcholine molecules have been reported to induce echinocytosis at a considerably lower level (16) but the cross-sectional area of their head groups are considerably larger than those of fatty acids and they possess moreover, two instead of one hydrocarbon chains. Incorporation of fatty acid probes or phospholipids is probably accompanied by loss of cholesterol and/or other lipids (16).

Evidence that fatty acid probes like PDA reside almost exclusively in the outer leaflet of the membrane comes from several sources. 1'-pyrene decanoic acid, which is expected to translocate in phospholipid bilayers at a faster rate than PDA, has been shown to remain in the outer leaflet at 32°C in a paramagnetic quenching study (17). Anthroyloxy stearic acid probes, which are similar to PDA, also do not translocate as was shown in a resonance energy transfer (RET) study involving a series of such probes (18). Human serum albumin (HSA) can extract fatty acids from the outer leaflets of erythrocytes (19) and we obtained unpublished experimental evidence that more than 96% of the PDA probes incorporated into red cells are extractable by incubation with HSA (2g/dl at 24°C for 10 min) at probe ratios of 0.25, even after the labeled cells had been previously incubated for 1 h at 37°C.

Finally, we performed experiments to measure the RET from the pyrene moiety of PDA to the cytoplasmic heme groups in red cells, to confirm that the probe was indeed in the outer lipid layer. The energy transfer efficiency was determined at a probe ratio of 5% by measuring the average lifetimes of PDA in the membranes of intact cells (τ_c) and in ghosts (τ_g) and by making use of the relationship (18, 19)

$$\frac{h_b}{d^3} = \frac{3.17 \times 10^6}{R_0^6}\left(\frac{\tau_g}{\tau_c} - 1\right), \qquad (1)$$

where d is the average normal distance from the hemoglobin boundary layer to the pyrene moiety and h_b is the heme concentration (in mM/l) in the cytosol hemoglobin boundary layer. With h_b = 15 mM/l and R_0 = 4.3 nm, assuming orientationally averaged RET (18, 19), and τ_c = 74 ± 5 ns and τ_g = 101 ± 5 ns, measured by means of a monophoton fluorescence decay instrument as described previously (18), one obtains d = 4.3 ± 0.7 nm. This average distance is consistent with the PDA probes being located primarily in the outer leaflet of the bilayer. Since τ_c was found to remain unchanged for PDA-labeled RBC over a period of 24 h at room temperature, one may conclude that the translocation of PDA to the inner leaflet is negligible in the course of our experiments.

The steady state emission anisotropy of PDA in intact cells and ghosts was found to be 0.025 ± 0.015 when excited at 340 nm at 21°C. When used in the Perrin equation (20), this low value of $\langle r \rangle$, together with a limiting anisotropy of ~0.2 and a lifetime of 74 ns leads to a value of ~10 ns for the rotational relaxation time of the pyrene moiety.

KINETICS OF EXCIMER PRODUCTION

Following his discovery of the red-shifted excimer emission and the identification of the molecular species from which it is emitted, Förster and his collaborators showed in a series of papers, that the excimer production rate of pyrene and similar organic molecules in organic solvents is diffusion limited (22–24). The relevant kinetic scheme may be written

$$A + h\nu \longrightarrow A^*$$

$$A + A^* \underset{k_d}{\overset{K}{\rightleftharpoons}} (AA)^*$$

$$A^* \xrightarrow{k_M, k'_M} A + h\nu_M$$

$$(AA)^* \xrightarrow{k_E, k'_E} 2A + h\nu_E,$$

[1] In a previous report (12) of lateral diffusion experiments using excimeric probes in the membranes of intact erythrocytes the probes were incorrectly identified as 1-pyrenehexadecanoic acid (PHD). It has now been established that, because of mislabelling by the supplier, these probes were in fact 1'-pyrenedodecanoic acid (PDA). We have repeated the earlier experiments with PDA and obtained diffusion coefficients within 10% of the earlier determination. PHD from two suppliers and positively identified by atomic analysis and chromatography was found to partition into membranes with much lower efficiency (~10×) than PDA, presumably because the longer fatty acid probes are less soluble in an aqueous medium and form micelles more readily.

where the dissociation rate of excimers, $(AA)^*$, is k_d, their radiative and nonradiative decay rates are k_E and k'_E, with k_M and k'_M the corresponding decay rates of excited monomers, A^*. $h\nu_M$ and $h\nu_E$ are monomeric and excimeric photons and K is the excimer formation rate which for the diffusion limited case is given by

$$K = k_a c, \tag{2}$$

where k_a is a second order association rate constant and c is the pyrene-probe concentration. The monomeric and excimeric quantum yields (ϕ_M, ϕ_E) are according to this kinetic scheme concentration-dependent and are defined by

$$\phi_M = \frac{k_M}{k_M + k'_M + K'} \tag{3}$$

$$\phi_E = \frac{k_E}{k_E + k'_E} \frac{K'}{k_M + k'_M + K'}. \tag{4}$$

The second factor of Eq. 4 represents the fraction of excited monomers that decay as excimers, either radiatively or nonradiatively. K' is the net excimer production rate,

$$K' = K \frac{k_E + k'_E}{k_E + k'_E + k_d}, \tag{5}$$

and approaches K when the dissociation rate of the excimer is negligible compared to its decay rate. This has been shown (22, 23) to be the case for pyrene excimers below 50°C.

At very low and very high concentrations, the quantum yields given by Eqs. 3 and 4 approach the "intrinsic" monomeric and excimeric quantum yields, defined by

$$\phi^*_M = \lim_{x \to 0} \phi_M(x) = \frac{k_M}{k_M + k'_M} \tag{6}$$

and

$$\phi^*_E = \lim_{x \to 1} \phi_E(x) = \frac{k_E}{k_E + k'_E}. \tag{7}$$

The concentration dependent monomer and excimer yields relative to their intrinsic yields are therefore

$$\frac{\phi_M}{\phi^*_M} = \frac{k_M + k'_M}{k_M + k'_M + K'} \tag{8}$$

and

$$\frac{\phi_E}{\phi^*_E} = \frac{K'}{k_M + k'_M + K'}. \tag{9}$$

In the diffusion-limited case (see Eq. 2) the relative quantum yields of Eqs. 8 and 9 have a particularly simple dependence on the concentration c,

$$\frac{\phi_M}{\phi^*_M} = \left(1 + \frac{c}{c_0}\right)^{-1} \tag{10}$$

and

$$\frac{\phi_E}{\phi^*_E} = \left(1 + \frac{c_0}{c}\right)^{-1}, \tag{11}$$

where c_0 is that concentration, for which the net excimer formation rate is equal to the monomer decay rate, i.e.,

$$c_0 = \frac{k_M + k'_M}{k_a} \frac{k_E + k'_E + k_d}{k_E + k'_E}. \tag{12}$$

The validity of Eq. 10 and 11 for pyrene in solution was established by experiment with c_0 for pyrene being ~1.2 mM/l in benzene (23) and 3.4 mM/l in *n*-octylalcohol (22). Note that with $k_d = 0$, Eq. 12 becomes

$$k_a c_0 = \tau_M^{-1}, \tag{13}$$

where $\tau_M = (k_M + k'_M)^{-1}$ is the monomer lifetime, measured at a sufficiently low probe concentration for the excimer formation rate to be negligible.

In discussing excimer kinetics of membrane probes it is convenient to express the probe concentration in terms of the molar probe fraction, x. Accurate excimer yields of excimeric pyrene probes in membranes can generally be obtained for probe ratios which are not much smaller than 0.01. The excimer production rate is expected to be diffusion-limited for sufficiently small values of x, but generally, the excimer production rate is best obtained from a simulation of the probes' motion within the membrane. In the model developed here and discussed in greater detail below, it is assumed that the excimeric probes are initially randomly distributed in a planar trigonal array of membrane lipids and that the probes' subsequent motion may be represented by spatial exchanges between the probe and one of its six nearest neighbor lipids, chosen at random. If this spatial exchange rate is ν and if p_E represents the probability that a nearest neighbor pair of probes, one excited and the other in its ground state, form an excimer in a time interval ν^{-1}, then the average number of such spatial exchanges that leads to the formation of an excimer is a function of x and p_E and is written $n(p_E, x)$. According to this model, the excimer formation rate is therefore

$$K = \frac{\nu}{n(p_E, x)}. \tag{14}$$

Using this in Eqs 3 and 4, with $k_d = 0$ the ratio of excimeric to monomeric quantum yield for any probe ratio, is given by

$$\frac{\phi_E(x)}{\phi_M(x)} = \frac{k_E}{k_M} \frac{\tau_E \nu}{n(p_E, x)}, \tag{15}$$

where $\tau_E = (k_E + k'_E + k_d)^{-1}$ is the excimer lifetime. Similarly, from Eqs. 6 and 7, the ratio of intrinsic quantum yields is

$$\frac{\phi^*_E}{\phi^*_M} = \frac{k_E}{k_M} \frac{\tau_E}{\tau_M} \tag{16}$$

so that, from Eqs. 15 and 16,

$$\frac{\phi_E(x)}{\phi_M(x)} = \frac{\phi_E^*}{\phi_M^*} \frac{\tau_M \nu}{n(p_E, x)}. \quad (17)$$

Instead of measuring absolute quantum yields, it is in general more convenient to measure two experimental parameters that are proportional to the monomeric and excimeric fluorescence yields,

$$J_M(x) = I_M(x)/x \quad (18)$$

and

$$J_E(x) = I_E(x)/x, \quad (19)$$

where $I_M(x)$ and $I_E(x)$ are the maximum intensities of the monomeric and excimeric fluorescence spectra. Since for any x, the ratio of quantum yields, $\phi_E(x)/\phi_M(x)$, is proportional to the yield ratio $J_E(x)/J_M(x)$ it is convenient to define the intensity ratio and its limiting value:

$$\rho(x) = \frac{J_E(x)}{J_M(x)} = \frac{I_E(x)}{I_M(x)} \quad (20)$$

$$\rho^* = \frac{J_E^*}{J_M^*}, \quad (21)$$

with

$$J_M^* = \lim_{x \to 0} J_M(x) \quad (22)$$

$$J_E^* = \lim_{x \to 1} J_E(x). \quad (23)$$

Substituting these parameters in Eq. 17,

$$\frac{\rho(x)}{\rho^*} = \frac{\tau_M \nu}{n(p_E, x)}. \quad (24)$$

Eq. 24 has the simple physical meaning that the ratio of fractional yields ($J_E(x)/J_E^*$, $J_M(x)/J_M^*$) for excimeric and monomeric emission is equal to the ratio of the excimer formation rate, $\nu/n(p_E, x)$, divided by the monomer decay rate (τ_M^{-1}). With $n(p_E, x)$ determined by means of computer simulations of an appropriate model and $\rho(x)$, ρ^* and τ_M determined by experiment, Eq. 24 may be used to estimate the spatial exchange frequency of the probes. The intensity ratio $\rho(x)$ may be measured with considerable precision as long as the monomeric and excimeric emissions are well resolved, as is the case for pyrene. ρ^* is obtained from the limiting values of the monomer and excimer yields at very low and very high probe ratios, respectively, (see Eqs. 22 and 23).

In practice, the excimer yield at very high probe ratios is sometimes difficult to measure and an analysis based on the monomer yield is preferable. From Eqs. 3 and 6, with $k_d = 0$, one obtains

$$\frac{\phi_M(x)}{\phi_M^*} = \frac{J_M(x)}{J_M^*} = \left[1 + \frac{\nu \tau_M}{n(p_E, x)}\right]^{-1}. \quad (25)$$

It follows from Eq. 25 that the monomer yield of excimeric probes drops to one half of J^* at a critical probe concentration x_c, for which the average time for excimer formation, $n(p_E, x_c)\nu^{-1}$ is equal to the monomer life time. Once x_c is determined in this manner, the experimental excimer yields may be fitted to Eq. 26, by an appropriate choice of J_E^* (see Eqs. 4 and 7 with $k_d = 0$)

$$\frac{\phi_E(x)}{\phi_E^*} = \frac{J_E(x)}{J_E^*} = \left[1 + \frac{n(p_E, x)}{\nu \tau_M},\right]^{-1}. \quad (26)$$

If k_n is the rate of excimer formation between nearest neighbor A and A^* probes, p_E can be expressed as

$$p_E = \frac{k_n}{k_n + k_M + k'_M} \quad (27)$$

so that

$$k_n = [(p_E^{-1} - 1)\, \tau_M]^{-1}. \quad (28)$$

Note that k_n depends on the dynamical structure of the probe and its lipid environment and is therefore expected to be temperature-dependent.

The details of the "milling crowd" model and how $n(p_E, x)$ is evaluated from it are given in the next section. Here we compare the predictions for the excimer/monomer intensity ratio and its dependence on the probe ratio for the milling crowd model and two others.

Diffusion Limit Model (DL)

This is analogous to Förster's original model for three-dimensional diffusion and is based on the assumption that excimer formation rate is proportional to the probe ratio x (see Eq. 2). Since not every encounter between A and A^* results in an excimer, the rate constant k_a is in reality the product of the collision frequency and the probability that the collision produces an excimer. In the two-dimensional problem considered here, the DL assumption is expected to be valid for very low probe ratios only, since the probability of two probes being nearest neighbors when one of them is excited, is then negligible. With pyrene-containing probes in membranes, however, such probe ratios result in negligibly small excimer production rates.

If the concentrations c and c_0 of Eq. 10 and 11 are expressed as the probe ratios x and x_0, and Eq. 11 is divided by Eq. 10, one obtains

$$\rho(x)/\rho^* = x/x_0. \quad (29)$$

In other words, $\rho(x)$ is a linear function of x, which passes through the origin and has a slope ρ^*/x_0. x_0 is as in Eq. 12 the probe ratio for which the excimer formation rate is equal to the monomer decay rate (see Eq. 13).

Random Walk Model (RW)

This model is based on the random walk of a probe among the lattice points of a square matrix, with the probe jump

frequency being ν_j. Galla and Sackmann and their collaborators, who developed this model (6, 8), set n_{RW}, the average number of jumps made by the probe before excimer is formed, equal to an asymptotic expression for the number of jumps made by an exciton before landing on an exciton trap. In this model the x dependence of $\rho(x)$ is, in analogy to Eq. 24, given by

$$\frac{\rho(x)}{\rho^*} = \frac{\tau_M \nu_j}{n_{RW}(x)}, \tag{30}$$

where

$$n_{RW}(x) = (2/\pi x) \ln (2/x) \tag{31}$$

is the asymptotic expression for infinitesimal x originally derived by Montroll for exciton migration in a square lattice (24). For a trigonal lattice, the appropriate expression is (24)

$$n_{RW}(x) = (\sqrt{3}/\pi x) \ln (2/x). \tag{32}$$

Note that in the RW model, an excimer is formed with unity efficiency when two probes formally "collide" on the same lattice point.

Milling Crowd Model (MC)

This model is considered to give a more realistic description of the kinetics of excimeric probes by postulating that probes migrate by changing places with membrane lipids at a particular frequency, with the excimerization probability between neighboring probes (p_E) providing a separate parameter. The average number of spatial exchanges that leads to the formation of an excimer is then a function of p_E and the probe ratio x and is determined by means of a computer simulation as described below.

THE MILLING CROWD MODEL

In this model the membrane phospholipids are assumed to form a regular trigonal array with probes occupying a fraction x of the lattice points. Each probe therefore has six nearest neighbors and migrates by changing places with a randomly chosen nearest neighbor, whether lipid or probe. These spatial exchanges take place at a frequency ν. The matrix used in the computer simulations of the probes' excimer production or diffusion rates has the shape of a regular trapezoid and had periodic boundary conditions, so that matrix points near the array's boundary had neighborhoods on two opposite edges. Experiments with arrays ($m \times m$) of different sizes showed that for $m \gtrsim 10$ the array size had surprisingly little effect on the simulated diffusibility of the probes, and 40×40 matrix was used in most cases. With it excimer production simulations in the presence of obstacles and with a low probe ratio ran several hundred seconds of Cray-1 time, while diffusion distance simulations of the kind described below, were ten times faster.

In an excimeric probe simulation employing an $m \times m$ matrix, the experiment begins by distributing xm^2 probes randomly. Of these, one randomly chosen probe was designated as an excited one (A^*), while the remaining $xm^2 - 1$ were ground state probes (A). Both A and A^* probes then underwent spatial exchanges with their neighbors and after each round, the six nearest neighbors of A^* were examined and the number of A neighbors were counted. If there was only one A, an excimer was formed with probability p_E. If there were q A's an excimer was formed with probability $1 - (1 - p_E)^q$. The formation of an excimer concluded an experiment and the number of iterations, $N_i(p_E, x)$ which had preceded the event was recorded. Otherwise the spatial exchange iterations continued until an excimer was formed. 100–1,000 iterations were typically sufficient but the number required clearly depends on p_E, x and any obstacles present in the matrix.

For obstructed diffusion simulations, hexagonic obstacles were distributed randomly over the matrix before each experiment (see Fig. 1). The side of the hexagons is $j\lambda$, where j is an integer and λ is the lattice spacing. The hexagons are allowed to touch, but cannot overlap each other. When a probe occupies a lattice point adjacent to an obstacle, a partner for an exchange is chosen at random as in the absence of obstructions, but if a lattice point is selected which is a part of an obstacle, no spatial exchange takes place for this probe, at least until the next round, when this procedure is repeated.

Histograms showing the probability distribution of $N_i(p_E, x)$, the number of exchanges leading to an excimer, are shown in Figs. 2*a*, 2*b*, and 2*c* for $p_E = 1$ and three probe ratios. The moments of such histograms give the average number of exchanges before an excimer is formed. This is $n(p_E, x)$, which is shown as a function of p_E and x in Fig. 3.

Since the MC and RW models have a formal resemblance and the latter has previously been used in the analysis of excimeric probe experiments (6, 8, 9), it is useful to compare their predictions. The RW model is based on exciton migration and therefore provides the numbers of steps before the probe arrives at a particular site (trap) and this event is considered equivalent to the formation of an excimer. The MC model with $p_E = 1$, on the other hand, yields the number of steps before a probe becomes one of six nearest neighbors of an excited probe. It is therefore not surprising that $n_{RW} \sim 6n(1, x)$, at least for small values of x. This results in the RW model yielding a jump frequency ν_j (and D) greater than the ν obtained by the MC model. If p_E is much less than unity, the probe is required to make many additional spatial exchanges before our excimer is formed, and with $p_E \sim 0.1$, the frequencies (and diffusion constants) obtained by the two models have similar values (see Fig. 3).

In principle, the validity of the MC model can be tested by comparing the measured monomer and/or excimer yields as functions of x, with the predictions of Eqs. 24, 25,

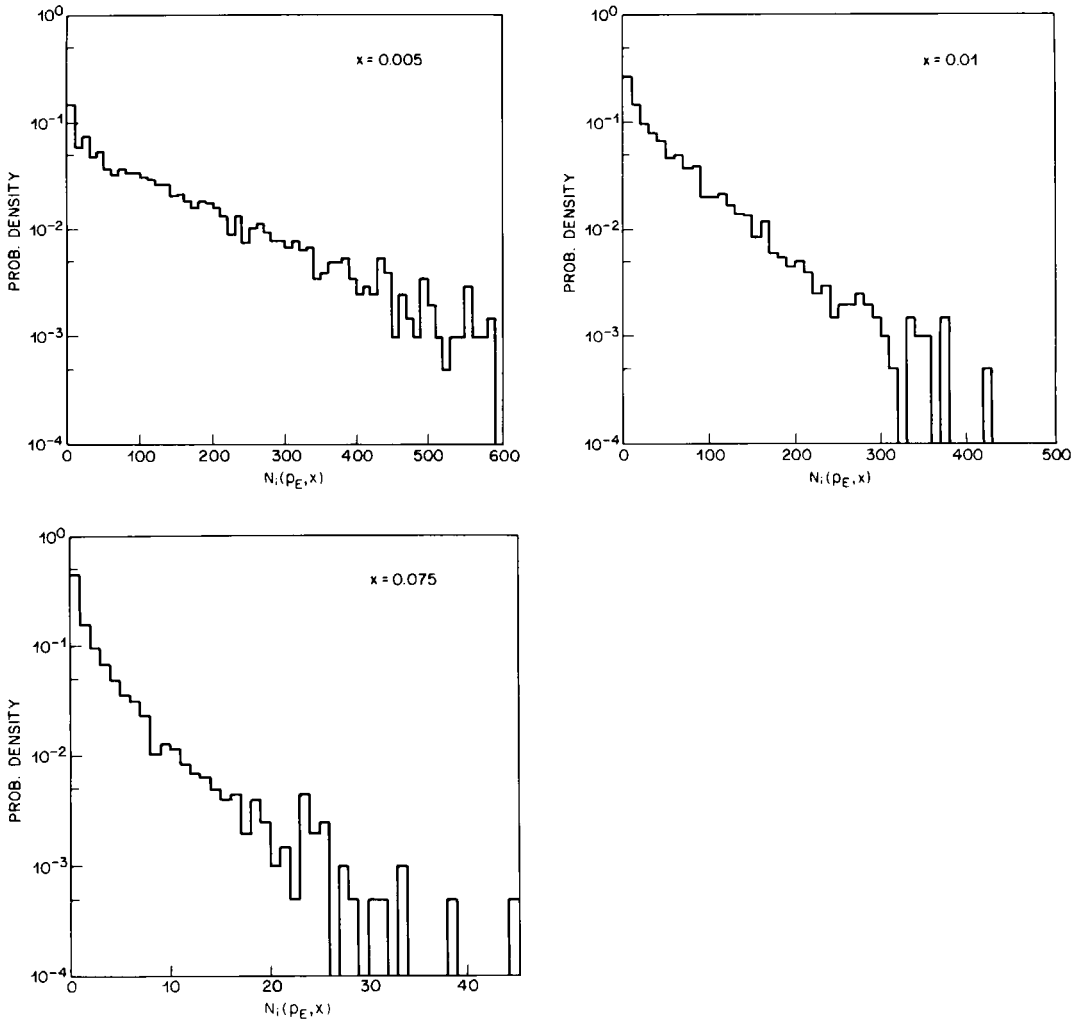

FIGURE 1 Illustrations of the regular trigonal array in which the lipids and probes are located with a random distribution of hexagonic obstacles ($j = 1$), covering a fractional area of $f = 0.21$.

and 26 and this is done in a later section. As can be seen from the x-dependence of $n(p_E, x)$ (see Fig. 3) it is possible to trade off p_E and ν to some extent at least for small x, since a higher exchange frequency can compensate for a reduced p_E. The MC model distinguishes between p_E and ν primarily when p_E and x are large ($p_E \sim 1$, $x \gtrsim 0.1$), because it is in this domain that one finds a significant contribution of static excimers, which are formed between neighboring probes in the absence of diffusion i.e. within ν^{-1}s of one of the probes being excited. Static excimers provide the explanation for the rapid decrease in $n(p_E, x)$ for large p_E and $x \gtrsim 0.1$ (see Fig. 3). The probability of static excimer formation, p_s, is readily seen to be the complement to the probability that a probe, upon excitation forms *no* excimers with its six neighbors in an interval ν^{-1}s. For the milling crowd model, therefore

$$p_s = 1 - (1 - p_E x)^6. \tag{33}$$

This exact expression is compared with the statistical results obtained by the computer simulated MC model in Fig. 4, and the agreement is seen to be good particularly for large x, for which better statistics were available.

If it is not possible to obtain excimeric and monomeric yields with sufficient precision to obtain the parameters p_E and ν independently, one may still determine the model-independent critical probe ratio x_c, at which the limiting monomeric yield is halved, i.e.

$$J_M(x_c) = J_M^*/2. \tag{34}$$

Since p_E cannot exceed unity, x_c may then be used to calculate a lower limit for the exchange frequency

$$\nu \gtrsim n(1, x_c)/\tau_M. \tag{35}$$

EXCHANGE FREQUENCY AND DIFFUSION COEFFICIENT

The diffusive (Brownian) motion of molecules is governed by the random fluctuations of the available thermal energy, $kT/2$. If molecules are confined to a plane and migrate a distance $d(t)$ by a random walk process, independently of

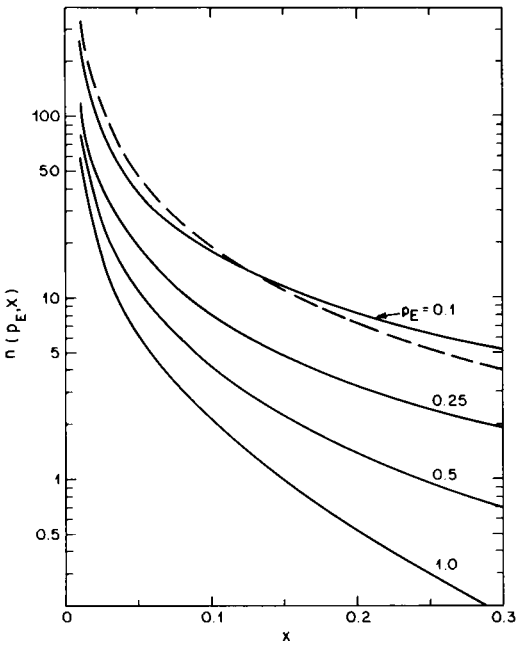

FIGURE 2 (a, b, c) Histograms showing the frequency distribution of the number of exchanges $N_i(p_E, x)$ which lead to the formation of an excimer with $p_E = 1$ and $x = 0.005, 0.02$, and 0.075. The average number of exchanges, $n(p_E, x)$, is the first moment of the probability density distribution and is 130, 24, and 3.5 for 1a, 1b, and 1c, respectively.

each other, and taking random steps in all directions at some frequency, it can readily be shown, that their root-mean-square displacement is proportional the square root of the time (25). The diffusion equation for two dimensions is usually written as

$$\langle d^2(t)\rangle = 4Dt, \tag{36}$$

where D is the lateral diffusion coefficient. The coefficient of t is $2D$ and $6D$ for diffusion in one and in three dimensions, respectively. According to the MC model, t can be expressed as $i\nu^{-1}$, where i is the number of spatial exchanges which take place at a frequency ν. $\langle d^2(i)\rangle$ may then be obtained by a computer simulation (see Section VII) and when plotted against i, one indeed obtains a straight line (see Fig. 8), whose slope may be set equal to $4D$ (see Eq. 36). This definition of D (see Eq. 36) can easily be shown to be consistent with differential form of the

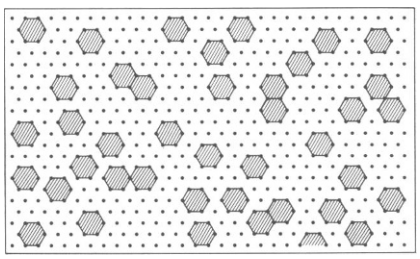

FIGURE 3 The x-dependence of $n(p_E, x)$ for p_E between 0.1 and 1. Note that $n(p_E, x)$ decreases more rapidly with x for large values of p_E, because of the contribution of static excimers (see text).

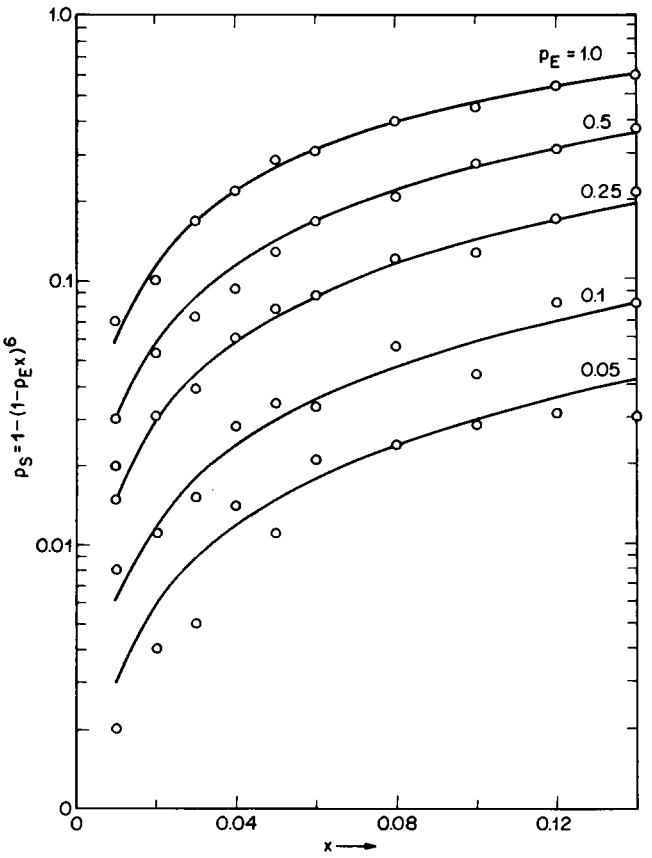

FIGURE 4 The x dependence of the probability of static excimers p_s for p_E between 0.05 and 1. The exact expression $p_s = 1 - (1 - p_E x)^6$ is shown by the curves while the values obtained in a computer simulation of the MC model are shown as circles.

diffusion (Fick's) equation (25)

$$J = -D \nabla c, \tag{37}$$

which states that the particle flux vector J is proportional to the negative particle concentration gradient, with D the proportionality constant. Eq. 37 is employed in the theoretical analysis of FPR experiments (3) so that the values of D obtained in that way equals, according to Eq. 36, a quarter of the slope of the mean-square distance vs. time or i

$$D = \frac{\nu}{4}[\langle d^2(i)\rangle - \langle d^2(i-1)\rangle]. \tag{38}$$

In a single spatial exchange a probe moves one lattice constant (λ) in a time ν^{-1}. It follows from Eq. 36 that the exchange frequency ν obtained from excimerization experiments is related to the diffusion coefficient according to (25, 26)

$$D = \nu\lambda^2/4. \tag{39}$$

COMPARISON WITH EXPERIMENT

In this section we illustrate how steady state measurements of the excimeric and monomeric emission intensities are

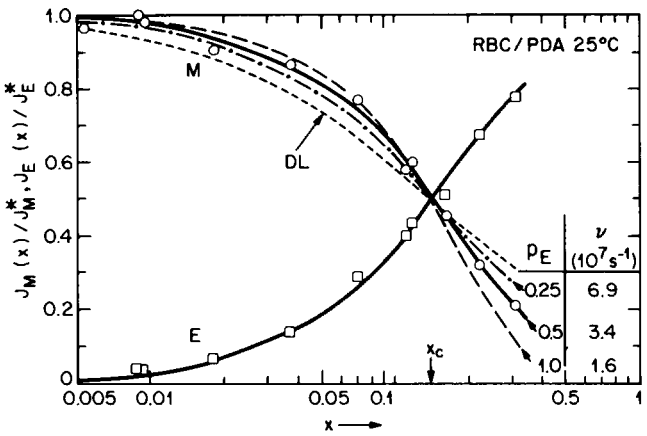

FIGURE 5 The x-dependence of the monomeric and excimeric emission intensity of PDA probes in the membrane of intact erythrocyte, compared to "best fit" theoretical curves according to the diffusion limited model (----) and the milling crowd model with p_E 1, 0.5, 0.25, corresponding to ν = 1.6, 3.4, and 6.9 × 10^7 s^{-1}, respectively.

used to obtain D and k_n, two parameters that characterize the probe/lipid dynamics of a membrane. The system used are intact human erythrocytes, for which lateral diffusion measurements by FPR exist (27). Excimeric probe experiments have because of the intense scattering and absorption of red cells been seriously hampered by these artifacts, but a simple protocol which corrects errors arising from them was recently reported and was employed for the fluorometric measurements reported here (13).

The monomeric-and excimeric yields $J_M(x)$ and $J_E(x)$ for PDA embedded in the outer leaflet of erythrocytes were measured for probe ratios between 0.005 and 0.3. At low x-values $J_M(x)$ reaches an asymptotic value, J_M^*, which can be determined with good accuracy (~10%) and Fig. 5 shows the normalized values of $J_M(x)/J_M^*$. The critical probe concentration is seen to be $x_c = 0.14$ and provides an easily measured, model-independent parameter indicative of the average local fluidity. The experimental error in the determination of x_c is estimated to be ±20 percent. According to Fig. 2, this corresponds to an error of ~50% in ν, if the uncertainty in τ_M is included.

In order to interpret x_c in terms of parameters used to characterize the dynamical properties of a probe/membrane system, it is necessary to relate it to a particular model. According to the diffusion-limited model with τ_M = 74 ns, is $k_a = 9.6 \times 10^7$ s^{-1} and the effective association rate represents, as noted above, a lower limit for the "collision" rate. From the theoretical x-dependence of $J_M(x)/J_M^*$ (see Eq. 10) shown in Fig. 5, it appears that the x-dependence of the experimental monomer yield is appreciably steeper than predicted by the DL model.

The experimental data of Fig. 5 are next compared to the predictions of the MC model (see Eq. 25). With x_c determined (see Eq. 34), one obtains the exchange fre-

TABLE I
DIFFUSIVITY PARAMETERS FOR PDA IN ERYTHROCYTE MEMBRANES COMPARED WITH OTHER PROBE AND MEMBRANE SYSTEMS

	System membrane*	Probe†	Method	p_E	k_n ($10^7 s^{-1}$)	ν ($10^7 s^{-1}$)	D ($10^{-9} cm^2 s^{-1}$)	Reference
				≲1	≳10	≲1.6	≲26	
1	Erythrocyte	PDA	Excimer	0.5	1.4	3.4	54	This work
				0.25	0.45	6.9	110	
				0.1	0.15	16	256	
2	Erythr. ghost	PDeA	Excimer§	(1)	—	16	256	(9)
3	Erythrocyte	dil	FPR	—	—	—	8	(28)
4	Erythr. ghost	dil	FPR	—	—	—	2	(36)
5	Erythr. ghost	dil	FPR	—	—	—	1.5	(35)
6	Fluid DMPC	dil	FPR	—	—	—	16–60	(33, 34)
7	Lymphocyte PM	dil	FPR	—	—	—	17	(38)
8	IMM	dil	FPR	—	—	—	5	(39)
9	DMPC, P/L = 0.05	diO	FPR	—	—	—	69	
10	DMPC, P/L = 0.07	diO	FPR	—	—	—	43	(37)
11	DMPC, P/L = 0.11	diO	FPR	—	—	—	25	
12	DMPC, P/L = 0.33	diO	FPR	—	—	—	7.3	

Comparison of local and long-range diffusibilities of lipid probes obtained by excimeric probes and FPR experiments. The experimental error in the determination of x_c is estimated to be ±20%, which leads to an uncertainty of ~50% in ν and D. This does not include the uncertainty due to the proper choice of p_E, which is discussed in the text.

*All experiments between 21°C and 25°C, except T = 35°C for systems 2 and 32°C for systems 9–12. DMPC: dimyristoylphosphatidylcholine vesicles. PM: plasma membrane. IMM: Inner mitochondrial membrane. P/L: molar bacteriorhodopsin/lipid ratio. The intra membrane particle density of systems 7 and 8 are estimated to be 500 and 5,300 and that of 3, 4, and 5 is 4,200 per μm^2 (see reference 29).

†PDeA: pyrene decanoic acid. DiO: dioctadecyloxatricarbocyanine iodide.
Dil: dioctaelecylindodicarbocyanine iodide.

§ν_j and D obtained by RW model analysis with the implicit assumption p_E = 1. See text.

quency by making use of the data of Fig. 3 and the relationship

$$\nu = n(p_E, x_c)/\tau_M. \quad (40)$$

With the experimental value for τ_M, Eq. 40 provides estimates for ν corresponding to different assumptions for p_E, and these are listed in Table I. For each of these, Fig. 5 shows the x-dependence of the monomer yield according to Eq. 25. While the other solutions cannot be discarded, the best fit is obtained with $p_E = 0.5$. This corresponds to $n(p_E, x) = 2.6$ and $\nu = (3.4 \pm 1.7) \times 10^7\ s^{-1}$. According to Eq. 28 the nearest neighbor excimerization rate k_n is therefore $1.4 \times 10^7\ s^{-1}$. The error in the determination of k_n due to the uncertainty in p_E is large, as can be seen by differentiation of Eq. 28 or from the p_E-dependence of ν shown in Table I.

If the quality of the experimental data does not warrant the selection of a particular p_E value, one may nevertheless obtain a valid lower limit for the probe/lipid exchange frequency by assigning p_E its maximum value (see Eq. 35): With $p_E \lesssim 1$, therefore, $\nu \gtrsim 1.6 \times 10^7\ s^{-1}$, so that this conservative data analysis yields a lower limit of 2.6×10^{-8} $cm^2\ s^{-1}$ for D.

In this analysis we used the $n(p_E, x)$ for unobstructed diffusion (see Fig. 2). In the presence of obstructions, $n(p_E, x)$ is increased by an amount that depends on the size and number of obstructions (see Fig. 7). It should be noted that if $n(p_E, x)$ values for obstructed diffusion had been employed in the analysis of the experimental yields, considerably greater diffusion coefficients (including the lower limit for $p_E \leq 1$) would have been derived.

It is more difficult to obtain reliable experimental values for J_E^* than for J_M^* because pure excimeric emission spectra must be measured at very high probe ratios. J_E^* was therefore determined by chosing a value that, when used to normalize $J_E(x)$, provides the optimum fit to experiment, using the same P_E and ν values as were obtained from an analysis of the monomeric yields. It can be seen that with $J_E^*/J_M^* = 0.88$, this procedure leads to an excellent agreement between theory and experiment with $p_E = 0.5$ and $\nu = 3.4 \times 10^7\ s^{-1}$ (see Fig. 5).

One may finally use the J_M^* and J_E^* values obtained as indicated above and compare the experimental, normalized excimer/monomer emission intensity ratio with the prediction of the milling crowd model according to Eq. 30. This comparison is shown in Fig. 6, which contains theoretical MC curves for different p_E values, as well as that for a diffusion-limited model. The $p_E = 0.5$ curve is seen to provide the best fit to the data.

The lateral diffusion coefficients calculated according to Eq. 39 with $\lambda \sim 0.8$ nm are shown along with ν and k_n values corresponding to different p_E's, in Table I. The table also shows experimental diffusion coefficients for intact erythrocytes and ghosts obtained in fluorescence photobleaching recovery experiments and it can be seen that

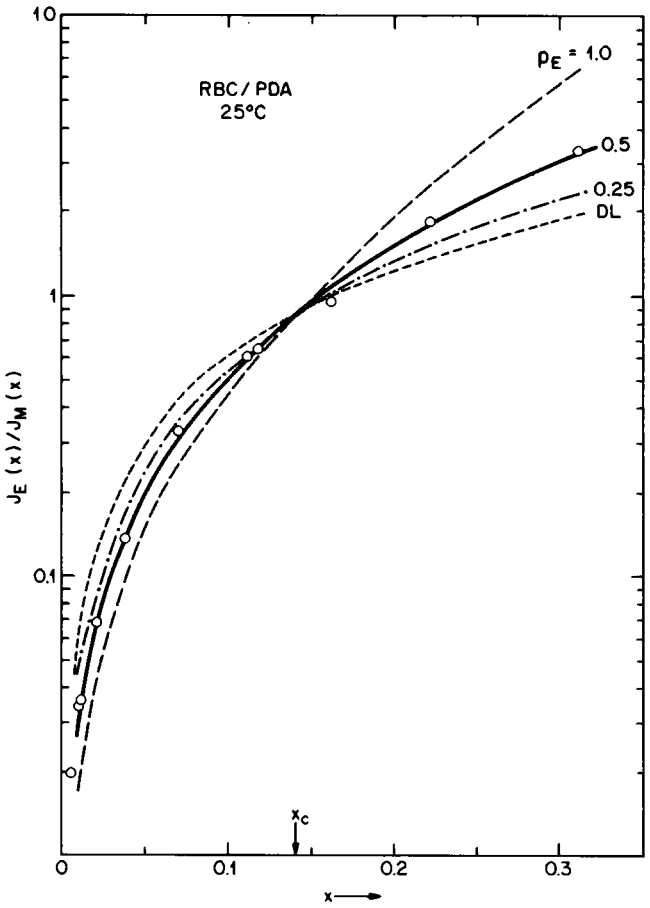

FIGURE 6 The excimeric/monomeric intensity ratio, $J_E(x)/J_M(x)$, normalized by the asymptotic yield ratio J_E^*/J_M^* as a function of the probe ratio x. The experimental points are for PDA probes in the membrane of intact erythrocytes at 21°C, and the theoretical curves for the DL and MC models are the same as those given in the caption of Fig. 4. The best fit gives $p_E = 0.5$, $\nu = 3.4 \times 10^7\ s^{-1}$.

even for the conservative assumption for p_E ($p_E \lesssim 1$), the local diffusion constant obtained by means of excimeric probes, is several times larger than that for long range diffusion, determined by FPR. For $p_E \sim 0.5$ and the x-range employed in the present experiments (0.005–0.3), $n(p_E, x)$ is of the order of 10, corresponding to a diffusion length of a few nm, while the diffusion distance is of the order of a μm for the FPR experiments. This distance is large enough to include many membrane proteins that obstruct long range diffusion of a lipid analogue membrane probe. The effect of obstacles on the probe's diffusibility is discussed in the next section.

OBSTRUCTED DIFFUSION

Most biological membranes consist of a bilayer of several different classes of lipids, in which are embedded a variety of integral proteins, some of which are immobilized by being associated with a polymeric network of cytoplasmic peripheral proteins, called the cytoskeleton. The fractional

membrane area that is occupied by proteins is approximately the same as the dry weight fraction and ranges from 20% for myelin to 75% for the purple membrane of *Halobacterium halobium* and the inner mitochondrial membrane (28-30). The lateral mobility of a lipid or a lipid analogue probe is expected to be reduced by the presence of dispersed membrane proteins, whose diffusibility is, because of their greater mass, considerably smaller, even if they are not anchored to the cytoskeleton (10, 31).

Here we generalize the milling crowd model by providing for the presence of forbidden regions or obstructions in the trigonal array of lipids that represents the membrane. These obstructions are here, for the sake of convenience, assumed to be hexagonal in shape, the hexagons' having sides of length $j\lambda$, where λ is taken to be equal to the average lipid-lipid separation. A random distribution of obstructions may then be characterized by the fractional area covered by obstacles (f), and by j (see Fig. 1).

Note that this model makes the following assumptions, whose validity for real membranes holds of course only approximately:

(*a*) Proteins are randomly distributed in a trigonal array of lipids that participate in spatial exchanges. They may touch (osculate) along their sides or vertices. They cannot overlap, however.

(*b*) The proteins are uniform in shape and size and stationary. Their area is calculated according to some chosen model (see below).

Since obstructions reduce the effective range of diffusing probes, fewer lattice sites are visited and the excimeric probes are less likely to become nearest neighbors for a given number of spatial interchanges, i. The average number of steps leading to an excimer $n(p_E, x)$ is therefore increased compared to the case of unobstructed diffusion and this is borne out by the results of milling crowd simulations shown in Fig. 7.

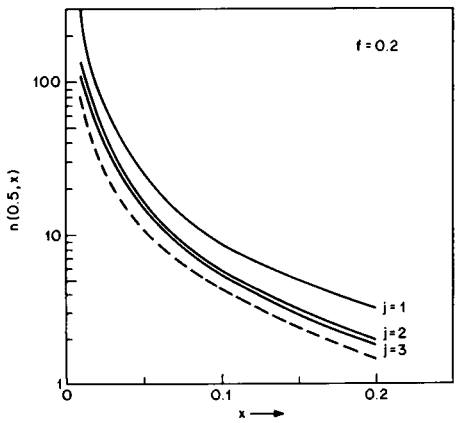

FIGURE 7 The effect of obstructions on the excimer production rate is here illustrated by MC simulations for $p_E = 0.5$. The fractional area of the lipid matrix covered by obstacles is $f = 0.2$. The obstructions are hexagons whose sides are $j\lambda$ in length. The dashed curve represents free diffusion. Note that the smallest obstructions ($j = 1$) cause the greatest increase in $n(p_E, x)$ (see Table I).

The effect of obstructions on long-range diffusion are, however, best demonstrated in the dependence of the computer-simulated mean-square-diffusion distance, $\langle d^2(i)\rangle$, on the number of probe-lipid exchanges, i (see Eq. 38). A probe was initially positioned in the center of a 40 × 40 lipid matrix and the distance it migrated following i spatial exchanges with randomly chosen nearest neighbors, was determined for a particular area coverage, obstacle size and i by 2,000 trials. Periodic boundary conditions were used as before and the positions of the obstructing hexagons were randomized for successive experiments. The results for these simulations are shown in Figs. 8 to 11 for a range of obstacle sizes and fractional area coverage of obstacles of f = 0.1, 0.2, 0.3, and 0.4 (see below for definition of f). Not surprisingly, a random distribution of small obstacles is seen to inhibit diffusion more effectively than do larger obstacles that cover the same fractional area. This is because small obstacles produce more small interstices between them, which effectively trap probes. In the limit when there are only a few very large obstacles, their effect becomes negligible.

When the mean-square-diffusion distance is plotted against the number of exchanges i, in the absence of obstacles one obtains as shown in Figs. 8–11 a straight line, in accord with the diffusion equation (see Eq. 36). If obstacles are present, this linear relationship no longer obtains and the diffusive behavior is best discussed by considering three regions of i: For very small values of i, or diffusion time, if the distance traversed by a probe is smaller than the average separation between obstacles, the diffusion coefficient is little changed from the obstacle-free

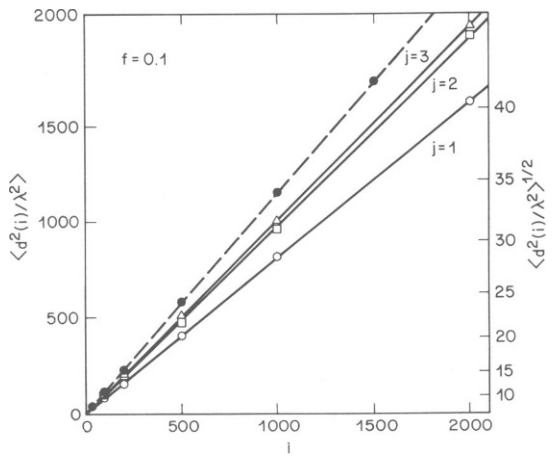

FIGURE 8 The mean square diffusion distance as multiple of the lattice constant, $\langle d^2(i)/\lambda^2\rangle$, as a function of i, or time, for a random distribution of hexagonal obstacles covering a fractional area (f) of 0.1 of the lipid matrix, obtained by milling crowd simulation. The right hand scale gives the root mean square diffusion distance. The dashed curve corresponds to unobstructed lateral diffusion and is a straight line, as expected from the diffusion equation (Eq. 36). Note that in the presence of obstacles, in the limit of large i, the curves are straight, as for unobstructed diffusion but the slope which is proportional to the effective lateral diffusion constant (D) is reduced, when compared to "free" diffusion (D_o).

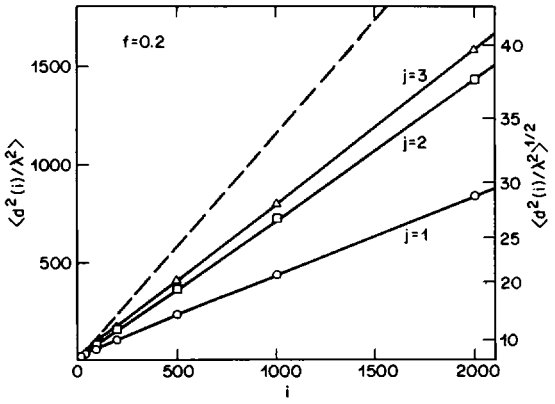

FIGURE 9 Same as Fig. 8, but for $f = 0.2$.

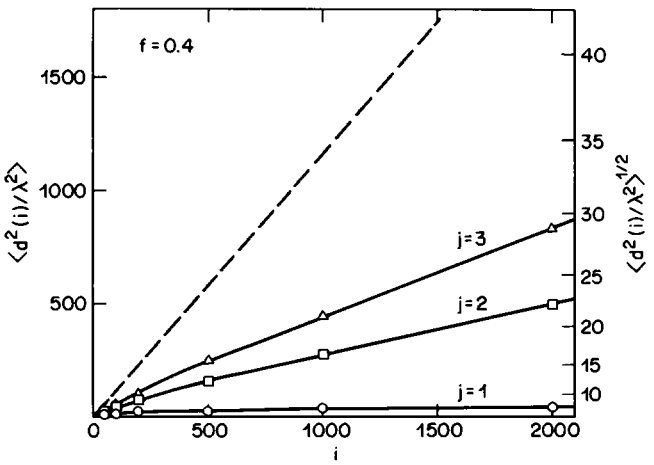

FIGURE 11 Same as Fig. 8, but for $f = 0.4$.

case. For large values of i, or long times, the mean-square diffusion distance in the presence of obstacles is proportional to i as it is for free diffusion, but with a reduced slope. In other words, the probes' motion is diffusive, but with a reduced diffusion coefficient. Between these two domains the effective diffusion constant has intermediate values and the probes motion is nondiffusive (see Fig. 12).

It is useful to present the effective, long-range diffusion coefficients obtained in this manner as a function of obstacle size and the fractional area covered by the obstacles. It is then necessary to choose among several possible ways of defining obstacle area, two of which are illustrated in Fig. 13 for $j = 1$ obstacles. In the model shown on the left and employed in Figs. 8–12, the obstacle area, A_T, is taken to be the hexagon's area, measured as the number of equilateral triangles with side λ (i.e. 6, 24, and 54 for $j = 1, 2, 3$ hexagons). The fractional area f is then defined by the sum of A_T for all obstacles, divided by the total area. Note that for this model the obstacle has six exchangeable nearest neighbors at a distance $\sqrt{3}\,\lambda/2$ (~0.7 nm).

On the right of Fig. 13 is shown an alternative model, in which the obstacle is surrounded by the same assembly of exchangeable lipids as in that shown on the left, but in considerably more intimate contact with them. Each lattice point is considered to be surrounded by an elementary hexagon that belongs either to an obstacle or the lipid matrix. For this model (but not for the model on the left) all space is occupied, so that the obstacle area is defined by the number of lattice points it contains (A_{LP}). (i.e. $A_{LP} = 7$, 19, and 37 for $j = 1, 2, 3$ obstacles). The fractional coverge, f_{LP}, is then obtained by dividing the sum of lattice points occupied by obstacles by the total number of lattice points. Since there exists a small overlap of areas when the hexagonic obstacles of the first model touch, the f_{LP} values obtained in this way represent overestimates, which are, however, small, at least for small and moderate f-values. This model postulates 12 nearest neighbor lipids at a distance of $\lambda/2$ from the perimeter (~0.4 nm). Not enough is known about lipid-protein interactions in membranes to decide which of these models is a more realistic one, but the existence of even a partial lipid solvation shell would favor the model on the left.

Table II shows the effect of obstacles on D, for different fractional coverages calculated according to both models.

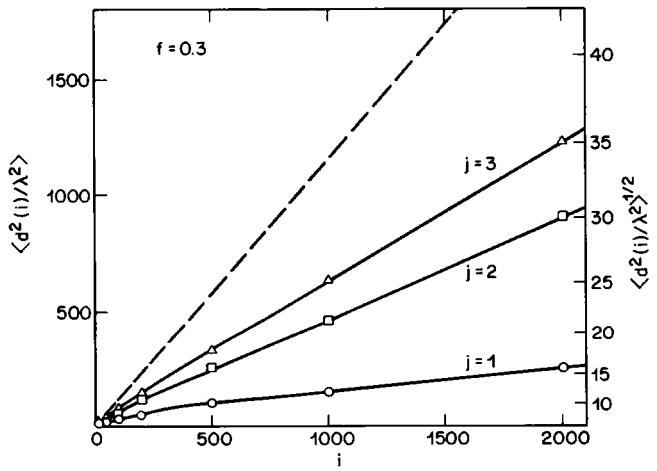

FIGURE 10 Same as Fig. 8, but for $f = 0.3$.

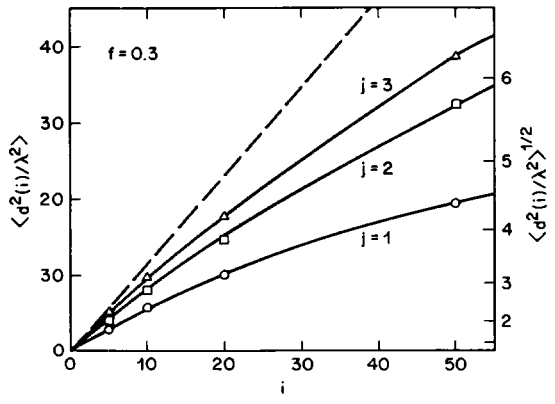

FIGURE 12 Same as Fig. 10, but for low and intermediate values of i. Note that in this regime the MC simulations do not satisfy Eq. 36 and the probes' mobility is not diffusive. The probes diffuse more rapidly locally when they remain between obstacles than over long distances.

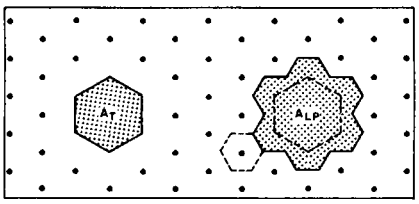

FIGURE 13 The lipid matrix surrounding $j = 1$ obstacles. The dots represent phospholipid or probe molecules that participate in random exchanges with their neighbors. The nearest neighbor lipids of the obstacle on the left are $\sqrt{3}\,\lambda/2$ or ~0.7 nm from its perimeter and it is surrounded by an empty annular region which can be thought of as containing a solvation shell of slowly exchanging lipid molecules. In the model to the right the lattice points are considered to be surrounded by elemental hexagons, each of which represents an exchangeable lipid or is part of an obstacle. The two models are used in the determination of the effective fractional area (f, f_{LP}) of obstacles in obstructed diffusion (see Fig. 14 *a*, *b*).

TABLE II
EFFECT OF OBSTACLES ON LONG-RANGE LATERAL DIFFUSION

	$j = 1$		$j = 2$		$j = 3$	
f	f_{LP}	D/D_0	f_{LP}	D/D_0	f_{LP}	D/D_0
0	0	1.00	0	1.00	0	1.00
0.1	0.23	0.70	0.16	0.80	0.14	0.81
0.2	0.47	0.35	0.32	0.62	0.27	0.68
0.3	0.70	0.09	0.48	0.38	0.41	0.52
0.4	0.93	~0	0.63	0.19	0.55	0.34
0.45	—	—	0.71	0.10	0.62	0.26

The lateral diffusion coefficient in the presence of randomly distributed hexagonal obstacles, as a function of the fractional area of the lipid matrix which is covered by obstacles. The fractional area is calculated according to the two models discussed in the text (f, f_{LP}). The listed values for D/D_0 are obtained from the limiting (high i) slopes of the milling crowd simulations shown in Figs. 8–11. j is the length of the hexagons' sides in terms of the matrix lattice constant, λ.

It is noteworthy that at sufficiently large coverage by small obstacles (e.g., with $f \sim 0.4$, $j = 1$), long-range diffusion becomes very unlikely and D becomes vanishingly small. The same data are presented graphically in Fig. 14, which shows the obstructed diffusion coefficient as a function of obstacle size and the fractional coverage. Note that the first model shows a considerably greater dependence on obstacle size than does the second one. The calculated obstacle size dependence of D depends critically on the method by which obstacle area is calculated and a comparison of Figs. 14 *a* and 14 *b* demonstrates that the simulated obstructed diffusion simulations are model-dependent. Thus the existence of a solvation shell, whose lipids exhibit a spatial exchange rate that is slow compared with that of the bulk lipid matrix, is expected to be an effective inhibitor of diffusion.

DISCUSSION

The local diffusion coefficient for a lipid analogue probe PDA in the erythrocyte membrane that is reported here ($D \gtrsim 3 \times 10^{-8}$ cm^2 s^{-1}) is of the same order of magnitude as that measured for long range diffusion of similarly sized probes in pure lipid multilayers, as measured by FPR experiments (29) (~2–6 $\times 10^{-8}$ cm^2 s^{-1}; see Table I). It is, on the other hand, considerably larger than the long-range (FPR) diffusion coefficients (2–8 $\times 10^{-9}$ cm^2 s^{-1}) for lipid probes in intact red cell membranes (28) and their ghosts (34, 35). Finally, since the average number of exchanges leading to an excimer is greater when the diffusion of the probes is obstructed (see Fig. 7) and the above results were obtained with an $n(p_E, x)$ for "free" diffusion, the local diffusion coefficient may well be appreciably larger than the values given above and in Table I. This would reinforce our contention that long-range diffusion is slowed severely by the presence of membrane proteins.

It has indeed been pointed out (31), that the diffusion coefficient of lipid analogue probes decreases by an order of magnitude when measured in systems containing increasing concentrations of membrane proteins. This is illustrated by typical results of FPR experiments using biological membranes and model membranes that contain different concentrations of intra-membrane particles, which are collected in Table I. Thus the long-range diffusion coefficient of a lipid probe in a vesicle system decreases by an order of magnitude when the bacteriorhodopsin/lipid ratio increases from 0 to 33% (36). These observations are consistent with the view that FPR experiments yield protein-obstructed diffusion coefficients, while excimeric probes report the local lateral fluidity of the membrane, which resembles that of pure lipid bilayers.

Table I also gives the jump frequency and diffusion coefficient reported by Galla and Luisetti for pyrene decanoic acid in erythrocyte membranes (9). Their analysis is based on the RW model which, as discussed in Section III, is expected to yield values of D which are considerably higher than the MC model analysis. The jump frequency reported by them for erythrocyte ghosts is comparable to those for several phospholipid vesicles and is at 35°C, 16×10^7 s^{-1}, corresponding to $D = 2.6 \times 10^{-7}$ cm^2 s^{-1}, an order of magnitude greater than the value obtained here by means of the MC model analysis.

According to our analysis probe-lipid exchanges occur at a rate $\nu \gtrsim 2 \times 10^7$ s^{-1}. It is noted that this frequency is of the same magnitude at the rate of rotation of PDA in the membrane, in accord with the milling crowd model in which spatial exchange and rotation are intimately connected. The spatial exchanges postulated in the milling crowd model are in any case not literally such: They represent rather, a convenient algorithm of a lateral displacement by a lipid-lipid spacing (~λ) in a random direction and they result from the random conformational fluctuations of the hydrocarbon chains in the bilayer.

The milling crowd analysis of excimeric probe studies yields the frequency ν (and hence D), but also provides an estimate for the nearest neighbor excimerization rate, k_n.

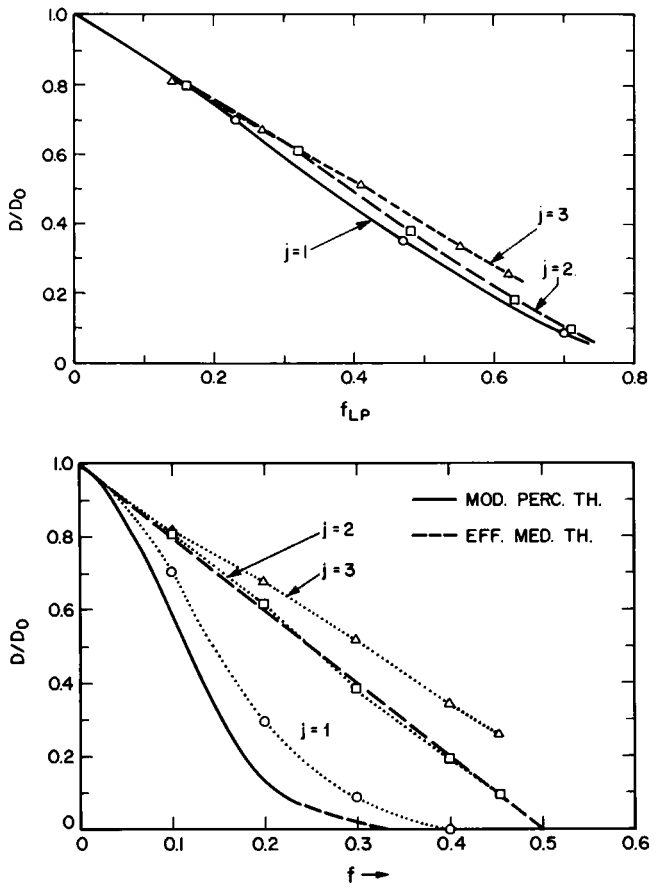

FIGURE 14 The lateral diffusion coefficient for obstructed lateral diffusion, D, normalized to the free diffusion coefficient D_0 as a function of obstacle size and density. The results of the MC simulation are shown for $j = 1, 2$, and 3 hexagons. The fractional area covered by the obstacles is calculated in two ways (f and f_{LP}); (*a*) corresponding to the model shown on the right of Fig. 13 and (*b*) as shown on the left side. (*b*) also shows the predictions of the effective medium theory (11) for obstructed diffusion (----) and of Saxton's modified percolation theory (11).

For PDA in erythrocyte membranes, $k_n \approx 1.4 \times 10^7\ s^{-1}$. The static excimer formation time is therefore ~70 ns, several times longer than the pyrene moieties' rotational relaxation time derived from the polarization of monomeric fluorescence (see Materials and Methods). This suggests that static excimerization can occur only, when the relative orientations of the pyrene moieties are within a limited range.

While ν provides a measure of the probes lateral diffusibility, k_n is indicative of the local membrane "fluidity." It is a more useful parameter than p_E, which is itself a function of ν.

The milling crowd simulations of the effects of obstructions on lipid diffusion suggest that the diffusion coefficients of biological membranes derived from photobleaching recovery experiments are, to a large extent, indicative of the number and sizes of the membrane proteins. An unexpected result of the simulations is that for the same fractional coverage, the diffusion coefficient is reduced to a much greater extent by small obstructions than by larger ones, at least for one of the models we have considered. In general, the magnitude of the size-dependence depends on the method by which obstacle area is calculated (see Table II and Figs. 13 and 14). The method used in Fig. 14 *a* shows a slight dependence on obstacle size while that of Fig. 14 *b* shows a very strong one. In contrast, the continuum theories of obstructed diffusion, which were recently reviewed by Saxton (11) and are discussed below, show no dependence on obstacle size. It is also clear from a consideration of the two models shown in Fig. 13, that solvation shells of slowly exchanging lipids can inhibit diffusion in an important way.

The existing two-dimensional diffusion theories were mostly developed for the calculation of the electrical conductivity of composite planar media, but diffusivity may be formally substituted for conductivity. The effective medium theories derive the effective conductivity in the presence of patches whose conductivity relative to that of the conductive phase is between 0 and 1 and predicts a particularly simple result if the obstacles are impermeable. For this case, if f is the fractional area occupied by obstacles, the effective diffusion coefficient is, according to Bruggeman (39) and Landauer (40)

$$D/D_0 = \begin{cases} 1 - 2f, f \le 1/2 \\ 0, f > 1/2 \end{cases} \qquad (42)$$

for a random distribution of circular obstacles. D_0 represents the lateral diffusion coefficient in the absence of obstacles. This theoretical result, which has been claimed to be insensitive to the sizes of the obstacles (11), is shown graphically in Fig. 14. Note that Eq. 42 predicts that long-range diffusion does not occur if f is greater than the critical ratio $f_c = 1/2$. For nonpermeable obstructions, the effective medium theory gives good approximations for small fractional areas, but for larger ones, the critical area predicted by percolation theory, $f_c = 0.322$, is generally considered appropriate (11). The results of continuum percolation theory are again independent of the size and shape of the obstacles, unless they are elongated or dendritic. It has been shown that in the vicinity of this f_c, a power law expression gives the dependence of the diffusion constant on the fractional area (41) and Saxton has proposed a semi-quantitative cubic function for the effective diffusion coefficient, which combines the results of the effective-medium and percolation theories in their respective domains of applicability (11). This function is shown in Fig. 14 *b*, along with the Bruggeman-Landauer equation, Eq. 42, and the results of the computer simulated milling crowd model.

Unlike the two continuum theories, the MC simulations for one of the models we have discussed show a strong dependence on obstacle size, particularly for small obstacles, i.e. those comparable to the lattice spacing (see Fig. 14). The $j = 1$ hexagons correspond to membrane particles

whose diameter is approximately 1.5 nm and this is comparable to the diameter of a gramicidin C dimer (1.2 nm), which has indeed been shown to affect long-range lipid diffusion profoundly (42). The critical area coverage, f_c, above which diffusion vanishes, depends on the obstacle size and falls, at least for $j = 1$, between the f_c predicted by the modified percolation theory (0.322) and that for the Bruggeman-Landauer equation (0.5). This suggests, that the long-range diffusion of lipid probes is critically dependent not only on the amount of intra-membrane particles, but on their distribution within the membrane. Model systems in which these effects can be determined experimentally are being studied and compared with MC simulations. These studies can also be extended to the diffusive behavior of membrane components of larger dimensions than lipids, e.g., proteins, in order to refine our understanding of the dynamic properties of biological membranes. The 1,000-fold range of measured long-range diffusion coefficients of membrane proteins (43) may be explainable by the wide range of protein densities which obtain in different membranes and perturb the effective D. It must be borne in mind however, that nondiffusive mobility e.g., flow, may also play a role.

It is noted that heterogeneities of membrane diffusibility that are produced, say, by heterogeneous distributions of membrane proteins, may play a role in the lateral transport of membrane components. The efficiency of such fluidity modulated mechanisms for membrane transport has recently been analyzed. J. Eisinger and B. I. Halperin (manuscript in preparation).

Only the steady state yields of excimeric probes are measured and analyzed in this paper. It should be noted however, that the probability distributions of $N_i(x)$ like the ones shown in Fig. 1 *a*, *b*, *c*, also represent the time dependence of the excimer formation rate, $K(t)$, in which the unit interval of the $N_i(p_E, x)$ axis corresponds to a time interval of ν^{-1} seconds. By determining $K(t)$ experimentally, it can be compared to milling crowd simulations as well as to theoretical predictions for the time dependence of such diffusion-controlled reactions between randomly distributed reactants (44). Such studies are expected to provide considerably more information about membrane fluidity than can be obtained from steady state experiments alone.

REFERENCES

1. Gupte, S., E-S. Wu, L. Hoechli, M. Hoechli, K. Jacobson, A. E. Sowers, and C. R. Hackenbrock. 1984. Relationship between lateral diffusion, collision frequency and electron transfer of mitochondrial inner membrane oxidation—reduction components. *Proc. Natl. Acad. Sci. USA.* 81:2606–2610.
2. Edidin, M. 1974. Rotational and translational diffusion in membranes. *Annu. Rev. Biophys. Bioeng.* 3:179–201.
3. Axelrod, D., D. E. Koppel, J. Schlessinger, E. Elson, and W. W. Webb. 1976. Mobility measurement by analysis of fluorescence photobleaching recovery kinetics. *Biophys. J.* 16:1055–1069.
4. Webb, W. W., L. S. Baiak, D. W. Tank, and E.-S. Wu. 1981. Molecular mobility on the cell surface. *Biochem. Soc. Symp.* 46:191–205.
5. Galla, H.-J., and E. Sackmann. 1974. Lateral diffusion in the hydrophobic region of membranes. Use of pyrene excimers as optical probes. *Biochim. Biophys. Acta.* 339:103–115.
6. Galla, H.-J., W. Hartman, U. Theilen, and E. Sackmann. 1979. On two-dimensional passive random walk in lipid bilayers and fluid pathways in biomembranes. *J. Mol. Biol.* 48:215–236.
7. Vanderkooi, J. M., and J. B. Callis. 1974. Pyrene. A probe of lateral diffusion in the hydrophobic regions of membranes. *Biochemistry.* 13:4000–4006.
8. Galla, H.-J., and W. Hartmann. 1980. Excimer-forming lipids in membrane research. *Chem. Phys. Lipids.* 27:199–219.
9. Galla, H.-J., and J. Luisetti. 1980. Lateral and transversal diffusion and phase transitions in erythrocyte membranes. An excimer fluorescence study. *Biochim Biophys. Acta.* 596:108–117.
10. Jacobson, K. 1983. Lateral diffusion in membranes. *Cell Mobility.* 3:367–373.
11. Saxton, M. J. 1982. Lateral diffusion in an archipelago. Effects of impermeable patches on diffusion in a cell membrane *Biophys. J.* 39:165–173.
12. Eisinger, J., J. Flores, and W. P. Petersen. 1985. A "Milling Crowd" Model for the lateral mobility of membrane probes. *Biophys. J.* 47 (2, pt. 2):366*a*. (Abstr.)
13. Eisinger, J., and J. Flores. 1985. Fluorometry of turbid and absorbant samples and the membrane fluidity of intact erythrocytes. *Biophys. J.* 48:77–84.
14. Sweeley, C. C., and G. Dawson. 1969. Lipids of the erythrocyte. *In* Red Cell Membrane. G. A. Jamieson and T. J. Greenwell, editors. J. B. Lippincott Co. 173.
15. Cooper, R. A. 1978. Influence of increased membrane cholesterol on membrane fluidity and cell function in human red blood cells. *J. Supramol. Struct.* 8:413–430.
16. Ferrell, J. E., Jr., L. Kong-Joo, and W. H. Huestis. 1985. Membrane bilayer balance and erythrocyte shape: a quantitative assessment. *Biochemistry.* 24:2849–2857.
17. Luisetti, J., H. Höhwald, and H.-J. Galls. 1979. Monitoring the location profile of fluorophores in phosphatidyl bilayers by the use of paramagnetic quenching. *Biochim. Biophys. Acta.* 522:519–530.
18. Eisinger, J., and J. Flores. 1983. Cytosol-membrane interface of human erythrocytes. A resonance energy transfer study. *Biophys. J.* 41:367–379.
19. Eisinger, J., and J. Flores. 1984. The cytosol-membrane interface of normal and sickle erythrocytes. Effect of hemoglobin deoxygenation and sickling. *J. Biol. Chem.* 259:7169–7177.
20. Lakowicz, J. R. 1983. Principles of Fluorescence Spectroscopy. Plenum Publishing Corp., New York. 134.
21. Förster, Th. 1969. Excimers. *Angew. Chem. Internat. Edit.* 8:333–343.
22. Döller, E., and Th. Förster. 1962. Der Konzentrationsumschlag der Fluoreszenz des Pyrens. *Z. Phys. Chem. N.F.* 34:132–150.
23. Förster, Th., and H.-P. Seidel. 1965. Untersuchungen zum Konzentrationsumschlags des Pyrens. *Z. Phys. Chem. N.F.* 45:58–71.
24. Montroll, E. W. 1969. Random walks on lattices. III. Calculation of first-passage times with application to exciton trapping in photosynthetic units. *J. Math. Phys.* 10:753–765.
25. Berg, H. C. 1983. "Random Walks in Biology." Princeton University Press, pp 5–21. The equivalence of the diffusion coefficient derived from a Markovian (random walk) process (Eq. 36) and from the classical diffusion equation (Eq. 37), was first established in 1906 by A. Einstein (see reference 45).
26. Devaux, P., and H. M. McConnell. 1972. Lateral diffusion in spin-labelled phosphotidylcholine multilayers. *J. Am. Chem. Soc.* 95:4475–4481.
27. Bloom, J. A., and W. W. Webb. 1983. Lipid diffusibility in the intact erythrocyte membrane. *Biophys. J.* 42:295–305.

28. C. W. M. Haest. 1982. Interactions between membrane skeleton proteins and the intrinsic domain of the erythrocyte membrane. *Biochim. Biophys. Acta.* 694:331–352.
29. Cohen, C. M. 1983. The molecular organization of the red cell membrane skeleton. *Sem Hematol.* 20:141–158.
30. Finean, J. B., and R. H. Michel. 1981. Membrane Structure. J. B. Finean and R. H. Michel, editors. Elsevier/North Holland, Amsterdam-NY-Oxford. 1–36.
31. Vaz, W. L. C., F. Goodsaid-Zalduondo, and K. Jacobson. 1984. Lateral diffusion of lipids and proteins in bilayer membranes *FEBS (Fed. Eur. Biochem. Soc.) Lett.* 174:199–207.
32. Derzko, Z., and K. Jacobson. 1980. Comparative lateral diffusion of fluorescent lipid analogues in phospholipid multilayers *Biochemistry.* 19:6050–6057.
33. Fahey, P. F., and W. W. Webb. 1978. Lateral diffusion in phospholipid bilayer membranes and multilamellar liquid crystals. *Biochemistry.* 17:3046–3053.
34. Thompson, N. L., and D. Axelrod. 1980. Reduced lateral mobility of fluorescent lipid probes in cholesterol-depleted erythrocyte membranes. *Biochim. Biophys. Acta.* 597:155–165.
35. Kapitza, H. G., and E. Sackmann. 1980. Local measurement of lateral motion in erythrocyte membranes by photobleaching technique. *Biochim. Biophys. Acta.* 595:56–64.
36. Peters, R., and R. J. Cherry. 1982. Lateral and rotational diffusion of bacteriorhodopsin in lipid bilayers: experimental test of the Saffman-Delbrück equations. *Proc. Natl. Acad. Sci. USA.* 79:4317–4321.
37. Dragsten, P., P. Hankart, R. Blumenthal, J. Weinstein, and J. Schlessinger. 1979. Lateral diffusion of surface immunogloblin Thy-1 antigen, and a lipid probe in lymphocyte plasma membranes. *Proc. Natl. Acad. Sci. USA.* 76:5163–5167.
38. Chazotte, B., E.-S. Wu, and C. R. Hackenbrock. 1983. The effect of varied membrane protein density on the lateral diffusion of lipids in the mitochondrial inner membranes. *Biochem. Soc. Trans.* 12:463–464.
39. Bruggeman, D. A. G. 1935. Berechnung verschiedener physikalischer Konstanten von heterogenen Substanzen. I. Dielektrizitatskonstanten aus isotropen Substanzen. *Ann. Phys. (Leipzig).* 24:636–679.
40. Landauer, R. 1978. Electrical conductivity in inhomogeneous media. *In* Electrical Transport and Optical Properties in Inhomogeneous Media. J. C. Garband and D. B. Tanner, editors. American Institute of Physics. New York. 2–45.
41. Kirkpatrick, S. 1976. Percolation and conduction. *Rev. Mod. Phys.* 45:574–588.
42. Tank, D. W., E. S. Wu, P. R. Meers, and W. W. Webb. 1982. *Biophys. J.* 40:129–135.
43. Edidin, M. 1981. Membrane Structure. J. B. Finean and R. H. Michel, editors. Elsevier/North Holland. Amsterdam-N.Y.-Oxford. 37–82.
44. Kang, K., and S. Redner. 1984. Scaling approach for the kinetics of recombination processes. *Phys. Rev. Lett.* 52:955–958.
45. Einstein, A. 1906. Zur Theorie der Brownschen Bewegung. *Ann. d. Physik.* 19:371–381.